MODELING, IDENTIFICATION AND CONTROL, 1984, VOL. 5, NO. 1, 47–70
doi:10.4173/mic.1984.1.3

General analysis of directional ocean wave data from heave/pitch/roll buoys

STEPHEN F. BARSTOW† and HARALD E. KROGSTAD†

Keywords: *ocean waves, wave analysis, buoy measurements, directional wave data.*

Directional ocean wave data is usually analysed using the so-called linear model of the sea surface, but experience has shown that the results may deviate substantially from the predictions of the theory, in particular in the high frequency range. A general theory is presented here which includes the linear model as a special case. Properties of commonly used parameters under the influence of currents and non-linearities are easily explained within the general theory. Some results from the NORWAVE heave/pitch/roll data buoy operated offshore Norway are also presented.

1. Introduction

Directional wave spectra are of considerable interest in current offshore and coastal engineering (Hogben 1982, Torset and Olsen 1982). For most applications the sea surface is treated as an infinite sum of non-interacting plane waves, each obeying the dispersion relation for infinitesimal waves. This is the so-called linear model. As a result of the dispersion relation, it is then possible to speak about a directional wave spectrum expressed only in terms of the wave number, or alternatively, frequency and direction. There exist various ways of measuring the directional spectrum, or at least, parts of it. However, it has frequently turned out that the data does not fit the linear model. This may be due to several reasons. Currents advect the waves and introduce a non-homogeneous dispersion relation, non-linearities present in the wave field introduce components that do not fulfil the dispersion relation, and finally, instrument imperfections further obscure the data interpretation. In the present paper we shall consider the sea surface under the general assumption of it being a homogeneous and stationary stochastic field and with special emphasis on observing the surface with a heave/pitch/roll buoy. Observed deviations from the linear model may be explained within the more general theory. In the next section we discuss stochastic models of the sea surface. We then consider the interpretation of the data from a heave/pitch/roll data buoy and in particular how commonly used parameters behave under the influence of currents and non-linearities. In later chapters some applications and results are presented from the NORWAVE data buoys which have been operating in the Norwegian Sea for the last three years.

2. Stochastic models of the sea surface

Let L^2 be a Hilbert space of real stochastic variables. For $X, Y \in L^2$ the expectation, EX, the covariance, $\mathrm{Cov}(X, Y) = E((X-EX)(Y-EY))$, and the variance, $\mathrm{Var}\, X = \mathrm{Cov}(X, X)$ have their usual meaning. A time varying stochastic surface $X(\boldsymbol{x}, t)$ is a

Received 14 February 1983.
† Continental Shelf Institute, P.O. Box 1883, 7001 Trondheim, Norway.

mapping from $R^2 \times R$ into L^2. The surface is mean square continuous at $(\boldsymbol{x}, t)$ if Var $(X(\boldsymbol{x}, t)-X(\boldsymbol{x}', t')) \to 0$ when $|\boldsymbol{x}-\boldsymbol{x}'| \to 0$ and $|t-t'| \to 0$. We shall assume that $E(X(\boldsymbol{x}, t))=0$. The surface is homogeneous if, for fixed t_1 and t_2, Cov $(X(\boldsymbol{x}_1, t_1), X(\boldsymbol{x}_2, t_2))$ is a function of $\boldsymbol{x}_2-\boldsymbol{x}_1$ only, and stationary if, for fixed $\boldsymbol{x}_1$ and $\boldsymbol{x}_2$, Cov $(X(\boldsymbol{x}_1, t_1), X(\boldsymbol{x}_2, t_2))$ is a function of t_2-t_1 only.

In the following we consider a zero mean, mean square continuous, homogeneous and stationary surface. This implies that the covariance function, $\rho_{XX}(\boldsymbol{x}, t)=$ Cov $(X(\boldsymbol{x}, t), X(\boldsymbol{0}, 0))$, is a continuous, even function. The surface also admits a spectral representation as follows

$$X(\boldsymbol{x}, t)=\int\int \exp(i(\boldsymbol{k}\cdot\boldsymbol{x}-\omega t))\, dZ(\boldsymbol{k}, \omega)$$

(Gihman and Skorohod 1980, p. 241). Integration without limits here and later is over wavenumber-frequency space. Z is the spectral amplitude of the surface and is an L^2-valued Borel measure, orthogonal on disjoint sets so that

$$E(Z(A))=0$$

$$E(Z(A)\overline{Z(B)})=0 \quad \text{if } A\cap B=\emptyset, \quad A, B\in\hat{R}^2\times\hat{R}$$

The positive measure χ defined by

$$\chi(A)=E(Z(A)\overline{Z(A)})$$

is the spectrum of X, and

$$\rho_{XX}(\boldsymbol{x}, t)=\int\int \exp(i(\boldsymbol{k}\cdot\boldsymbol{x}-\omega t))\, d\chi(\boldsymbol{k}, \omega)$$

Since X is real,

$$X(\boldsymbol{x}, t)=2\ \mathrm{Re}\left\{\int\int_{\omega>0} \exp(i(\boldsymbol{k}\cdot\boldsymbol{x}-\omega t))\, dZ(\boldsymbol{k}, \omega)\right\}$$

and

$$\rho_{XX}(\boldsymbol{x}, t)=2\int\int_{\omega>0} \cos(\boldsymbol{k}\cdot\boldsymbol{x}-\omega t)\, d\chi(\boldsymbol{k}, \omega)$$

The Fourier transform $\hat{f}$ of a function $f\in L^1(R^2\times R)$ is defined by

$$\hat{f}(\boldsymbol{k}, \omega)=\frac{1}{(2\pi)^3}\int\int \exp(-i(\boldsymbol{k}\cdot\boldsymbol{x}-\omega t))f(\boldsymbol{x}, t)\, dx_1\, dx_2\, dt$$

and may be extended to generalized functions in the usual way. Any generalized function h such that $\hat{h}\in L^2(\chi)$ introduces a linear operation on X by

$$h*X=\int\int \hat{h}(\boldsymbol{k}, \omega)\exp(i(\boldsymbol{k}\cdot\boldsymbol{x}-\omega t))\, dZ(\boldsymbol{k}, \omega)$$

For example, $\partial X(\boldsymbol{x}, t)/\partial t$ exists as the mean square limit of the integral

$$\int\int (-i\omega)\exp(i(\boldsymbol{k}\cdot\boldsymbol{x}-\omega t))\, dZ(\boldsymbol{k}, \omega)$$

if

$$\int\int |\omega|^2\, d\chi(\boldsymbol{k}, \omega)<\infty$$

Mean square existence does not necessarily imply pointwise derivatives.

For later use we also consider the operators $D_1=\partial/\partial x_1$ and $D_2=\partial/\partial x_2$. The Fourier transforms are $\hat{D}_1=ik_1$, $\hat{D}_2=ik_2$, where $\boldsymbol{k}=k_1\boldsymbol{i}+k_2\boldsymbol{j}$. Thus,

$$\begin{aligned}\rho_{D_1X,X}(\boldsymbol{x},t)&=E(\partial X/\partial x_1(\boldsymbol{x},t),X(0,0))\\&=\int\int ik_1\exp(i(\boldsymbol{k}\cdot\boldsymbol{x}-\omega t))\,d\chi(\boldsymbol{k},\omega)\\&=-2\iint\limits_{\omega>0}k_1\sin(\boldsymbol{k}\cdot\boldsymbol{x}-\omega t)\,d\chi(\boldsymbol{k},\omega)\end{aligned}$$

Similarly,

$$\left.\begin{aligned}\rho_{D_2X,X}(\boldsymbol{x},t)&=-2\iint\limits_{\omega>0}k_2\sin(\boldsymbol{k}\cdot\boldsymbol{x}-\omega t)\,d\chi(\boldsymbol{k},\omega)\\\rho_{D_1X,D_1X}(\boldsymbol{x},t)&=2\iint\limits_{\omega>0}k_1^2\cos(\boldsymbol{k}\cdot\boldsymbol{x}-\omega t)\,d\chi(\boldsymbol{k},\omega)\\\rho_{D_1X,D_2X}(\boldsymbol{x},t)&=2\iint\limits_{\omega>0}k_2^2\cos(\boldsymbol{k}\cdot\boldsymbol{x}-\omega t)\,d\chi(\boldsymbol{k},\omega)\\\rho_{D_1X,D_2X}(\boldsymbol{x},t)&=2\iint\limits_{\omega>0}k_1k_2\cos(\boldsymbol{k}\cdot\boldsymbol{x}-\omega t)\,d\chi(\boldsymbol{k},\omega)\end{aligned}\right\}\qquad(1)$$

Consider a homogeneous and stationary ocean. The sea surface elevation η and the fluid velocity potential Φ may be written as follows

$$\eta(\boldsymbol{x},t)=\int\int\exp(i(\boldsymbol{k}\cdot\boldsymbol{x}-\omega t))\,dB(\boldsymbol{k},\omega)$$

$$\Phi(\boldsymbol{x},z,t)=\int\int\exp(i(\boldsymbol{k}\cdot\boldsymbol{x}-\omega t))\,dA'(z,\boldsymbol{k},\omega)$$

(Mitsuyasu *et al.* 1979). If incompressible, inviscid and irrotational conditions are assumed and the depth is large, then

$$\nabla^2\Phi=0,\ z<\eta$$

and the free surface boundary conditions are

Kinematic condition: $\dfrac{\partial\eta}{\partial t}=\dfrac{\partial\Phi}{\partial z}-(\Phi_x\eta_x+\Phi_y\eta_y)$

Dynamic condition: $\dfrac{\partial\Phi}{\partial t}+\dfrac{1}{2}(\Phi_x^2+\Phi_y^2)+g\eta=0$

Moreover, $\Phi\xrightarrow[z\to-\infty]{}0$ (z is positive upwards).

From Laplace's equation it follows that

$$\Phi(\boldsymbol{x},z,t)=\int\int\exp(i(\boldsymbol{k}\cdot\boldsymbol{x}-\omega t))\exp(kz)\,dA(\boldsymbol{k},\omega),\ k=|\boldsymbol{k}|$$

and the kinematic and dynamic surface boundary conditions give to first order

$$\omega^2=gk$$

$$dA(\boldsymbol{k},\omega)=-\frac{i\omega}{k}\,dB(\boldsymbol{k},\omega)$$

The support of dB and dA is consequently, to first order, on the surface $\omega^2=gk$. The expansion to third order in mean wave steepness is given by Mitsuyasu *et al.* (1979), whereas an expansion to sixth order including only terms leading to energy

redistribution is found in Hasselmann (1962). The expansion is analogous to Stokes' expansion of finite amplitude waves and show that higher order terms give non-zero contributions away from $\omega^2=gk$ as well as a second order shift of the first order dispersion surface itself. We shall refer to the first order solution as the linear model. This is slightly more general than the model introduced by Longuet-Higgins (1956) who assumes that

$$\eta(\boldsymbol{x}, t)=\sum_i a_i \cos(\boldsymbol{k}_i \cdot \boldsymbol{x}-\omega_i t+\phi_i)$$

Here $\{\boldsymbol{k}_i\}$ is spread densely over the $\boldsymbol{k}$-plane, $\omega_i=(g|\boldsymbol{k}_i|)^{1/2}$, $\{\phi_i\}$ are independent random variables uniformly distributed on the interval $(0, 2\pi)$, and the amplitudes are positive random variables, mutually independent and also independent from ϕ_i.

When dB lies on $\omega^2=gk$ we may define the measure W on the $\boldsymbol{k}$-plane by $W(C)=B(C\times[0, \infty])$ and write

$$\eta(\boldsymbol{x}, t)=2\ \mathrm{Re}\left\{\int_{\boldsymbol{k}} \exp(i(\boldsymbol{k}\cdot\boldsymbol{x}-(gk)^{1/2}t)\, dW(\boldsymbol{k})\right\}$$

($C\times[0, \infty]$ is the cylinder ranging from $\omega=0$ to $\omega=\infty$ with base C.)

We shall denote

$$\Psi(C)=E(W(C)\overline{W(C)})=\chi(C\times[0, \infty]) \tag{2}$$

the wave number spectrum although this deviates from the definition in Phillips (1977). When Ψ is absolutely continuous, i.e. $d\Psi(\boldsymbol{k})=\psi(\boldsymbol{k})\, d\boldsymbol{k}$, $\psi\in L^1(\hat{R}^2)$, we may introduce polar coordinates and write

$$d\Psi(\boldsymbol{k})=\psi(k, \theta)k\, dk\, d\theta \tag{3}$$

Since $\omega^2=gk$, we also have

$$\begin{aligned}\psi(k, \theta)k\, dk\, d\theta&=\psi(\omega^2/g, \theta)\frac{2\omega^3}{g^2}\, d\omega\, d\theta\\&=S(\omega)D(\omega, \theta)\, d\omega\, d\theta\end{aligned} \tag{4}$$

where

$$\int_{-\pi}^{\pi} D(\omega, \theta)\, d\theta=1$$

The function $S(\omega)D(\omega, \theta)$ is usually called the directional wave spectrum, whereas S is the one dimensional wave spectrum or simply the spectrum.

We shall now consider the effect of a uniform current $\boldsymbol{U}$. Let $(\boldsymbol{x}', t')$ be the coordinates of a system which is moving with velocity $\boldsymbol{U}$, and $(\boldsymbol{x}, t)$ is a system remaining fixed. Thus,

$$\boldsymbol{x}=\boldsymbol{x}'+\boldsymbol{U}t'$$

$$t=t'$$

Assume that the surface in the moving system has the spectral representation

$$X'(\boldsymbol{x},' t')=\int\int \exp(i(\boldsymbol{k}'\cdot\boldsymbol{x}'-\omega' t'))\, dZ'(\boldsymbol{k}', \omega')$$

The same surface viewed from the system at rest is

$$\begin{aligned} X(\boldsymbol{x}, t) &= X'(\boldsymbol{x}-\boldsymbol{U}t, t) \\ &= \int\int \exp\,(i(\boldsymbol{k}'\cdot\boldsymbol{x}-(\omega'+\boldsymbol{k}'\cdot\boldsymbol{U})t))\, dZ'(\boldsymbol{k}', \omega') \\ &= \int\int \exp\,(i(\boldsymbol{k}\cdot\boldsymbol{x}-\omega t))\, dZ'(\boldsymbol{k}, \omega-\boldsymbol{U}\cdot\boldsymbol{k}) \\ &= \int\int \exp\,(i(\boldsymbol{k}\cdot\boldsymbol{x}-\omega t))\, dZ(\boldsymbol{k}, \omega) \end{aligned}$$

Thus, by virtue of the uniqueness of the spectral representation (Gihman and Skorohod 1980, p. 241)

$$dZ(\boldsymbol{k}, \omega) = dZ'(\boldsymbol{k}, \omega-\boldsymbol{U}\cdot\boldsymbol{k})$$

We may also show that

$$d\chi(\boldsymbol{k}, \omega) = d\chi'(\boldsymbol{k}, \omega-\boldsymbol{U}\cdot\boldsymbol{k})$$

The transformation may be visualized by considering χ' as a mass distribution. Obtaining χ from χ' is equivalent to moving slices (in $(\boldsymbol{k}, \omega)$ space) orthogonal to $\boldsymbol{U}$ vertically the amount $\boldsymbol{U}\cdot\boldsymbol{k}$. From (2) it follows that Ψ remains invariant as long as the support of χ does not intersect $\omega=0$. The latter case obviously corresponds to the flip in apparent propagation direction when $\boldsymbol{U}\cdot\boldsymbol{k}$ is larger than ω. The (symmetric) wave number spectrum defined by Phillips (1977) is completely independent of $\boldsymbol{U}$ in accordance with the fact that this spectrum may be obtained from an instantaneous observation of the surface (Phillips 1977, p. 102). The transformation of spectra in the case of the linear model is somewhat awkward since χ is singular, i.e. supported by the surface $\{(\boldsymbol{k}, \omega);\ \omega=\boldsymbol{U}\cdot\boldsymbol{k}-\sqrt{(gk)}$, or $\omega=\boldsymbol{U}\cdot\boldsymbol{k}+\sqrt{(gk)}\}$. A full treatment may be found in Kitaigorodskii *et al.* (1975), or Forristall *et al.* (1978). However, as long as the support of χ does not intersect $\omega=0$ we have

$$\begin{aligned} S(\omega)D(\omega, \theta)\, d\omega\, d\theta &= \psi(k, \theta)k\, dk\, d\theta \\ &= \psi(k(\omega, \theta), \theta)k(\omega, \theta)\frac{1}{|\partial\omega/\partial k|}\, d\omega\, d\theta \end{aligned} \tag{5}$$

where $\omega>0$, U is along the k_1-axis, θ is the angle between $\boldsymbol{U}$ and $\boldsymbol{k}$ and ω-$Uk\cos\theta-(gk)^{1/2}=0$ (Kitaigorodskii 1975, eqn. 2.4).

3. Directional parameters computed from heave/pitch/roll data

A floating buoy has six degrees of freedom: heave, sway, surge, yaw, roll and pitch. In the linear theory of buoy behaviour in a regular wave

$$\eta = \mathrm{Re}\,[A\exp\,(i(\boldsymbol{k}\cdot\boldsymbol{x}-\omega t))],$$

the complex amplitudes of the degrees of freedom $\{\xi_i\}_{i=1}^6$ are related to the wave force excitation coefficients $\{X_i\}_{i=1}^6$ by

$$\sum_{j=1}^{6} \xi_j(-\omega^2(M_{ij}+a_{ij})+i\omega b_{ij}+c_{ij}) = AX_i \tag{6}$$

(cf. Newman 1980. § 6.15 to 6.21).

The mass matrix $\{M_{ij}\}$ contains the mass and moments of inertia, $\{a_{ij}\}$ is the added mass matrix $\{b_{ij}\}$ the radiation and viscous damping, and $\{c_{ij}\}$ are the stiffness coefficients. The added mass and damping coefficients are in general dependent on ω. In a random sea one assumes that this relationship holds also for the spectral amplitudes. Below we consider buoys which are rotationally symmetric with respect to the vertical axis. Thus, the only cross-couplings that remain are sway–roll and surge–pitch (Newman p. 308). If the horizontal motions are neglected, eqn. (6) becomes completely decoupled and the relations between the buoy's heave, pitch and roll (β, β_x, β_y), and the sea surface are as follows:

$$\beta(t)=\int\int h(\omega)\exp(-i\omega t)\,dB(\boldsymbol{k},\omega)$$

$$\beta_x(t)=\int\int d_x(\omega)\exp(-i\omega t)\,(ik_x)\,dB(\boldsymbol{k},\omega)$$

$$\beta_y(t)=\int\int d_y(\omega)\exp(-i\omega t)\,(ik_y)\,dB(\boldsymbol{k},\omega)$$

where the buoy is situated at $\boldsymbol{x}=0$, and (h, d_x, d_y) are the transfer functions.

We find from eqn. (6) that

$$h(\omega)=\frac{X_h}{-\omega^2(M+a_{hh})+i\omega b_{hh}+c_{hh}}$$

where subscript h denotes heave. The relationships for d_x and d_y are similar. If mooring effects are negligible, then $d_x=d_y$.

The first step in analysing data records from the buoy is to form all auto and cross-spectra from $\beta(t)$, $\beta_x(t)$, and $\beta_y(t)$. Since, for example

$$\mathrm{Cov}\,(\beta_x(t),\beta(0))=\int_\omega \exp(-i\omega t)\,d\omega\left[id_x(\omega)\overline{h(\omega)}\int_k k_1\,d\chi(\boldsymbol{k},\omega)\right]$$

the phase of the cross-spectrum between β_x and β is equal to the phase of $id_x\bar{h}$. Moreover, the cross-spectrum between β_x and β_y should be real if $d_x=d_y$. In fact, for the NORWAVE buoy we shall see, in the next section, that these properties have been used in deriving the transfer function for pitch and roll. If we assume that the correct transfer functions have been found, the six auto and cross-spectra of β, β_x and β_y give us from eqn. (1) the following integral properties of the wave spectrum χ for each frequency $\omega>0$:

$$\left.\begin{aligned}
S_{hh}(\omega)&=\int_k d\chi(\boldsymbol{k},\omega)\\
S_{xh}(\omega)&=\int_k k_1\,d\chi(\boldsymbol{k},\omega)\\
S_{yh}(\omega)&=\int_k k_2\,d\chi(\boldsymbol{k},\omega)\\
S_{xx}(\omega)&=\int_k k_1^2\,d\chi(\boldsymbol{k},\omega)\\
S_{yy}(\omega)&=\int_k k_2^2\,d\chi(\boldsymbol{k},\omega)\\
S_{xy}(\omega)&=\int_k k_1k_2\,d\chi(\boldsymbol{k},\omega)
\end{aligned}\right\}\qquad(7)$$

For the special case of the linear model in deep water and with zero current, we obtain the following well known relations using eqns. (2), (3) and (4).

$$\left.\begin{aligned}
S_{hh}(\omega) &= S(\omega)\int_0^{2\pi} D(\omega,\theta)\,d\theta = S(\omega)\\
S_{xh}(\omega) &= S(\omega)\frac{\omega^2}{g}\int_0^{2\pi}\cos\theta D(\omega,\theta)\,d\theta\\
S_{yh}(\omega) &= S(\omega)\frac{\omega^2}{g}\int_0^{2\pi}\sin\theta D(\omega,\theta)\,d\theta\\
S_{xx}(\omega) &= S(\omega)\frac{\omega^4}{g^2}\int_0^{2\pi}\cos^2\theta D(\omega,\theta)\,d\theta\\
S_{yy}(\omega) &= S(\omega)\frac{\omega^4}{g^2}\int_0^{2\pi}\sin^2\theta D(\omega,\theta)\,d\theta\\
S_{xy}(\omega) &= S(\omega)\frac{\omega^4}{g^2}\int_0^{2\pi}\cos\theta\sin\theta D(\omega,\theta)\,d\theta
\end{aligned}\right\} \tag{8}$$

(Longuet-Higgins *et al.* 1963, Borgman 1979).

The conventional procedure is now to consider the Fourier series of D,

$$D(\omega,\theta)=\frac{1}{2\pi}\left[1+2\sum_{n=1}^{\infty}\{a_n(\omega)\cos(n\theta)+b_n(\omega)\sin(n\theta)\}\right]$$

from which it follows that

$$\left.\begin{aligned}
a_1(\omega) &= S_{xh}(\omega)/(S(\omega)\omega^2/g)\\
b_1(\omega) &= S_{yh}(\omega)/(S(\omega)\omega^2/g)\\
a_2(\omega) &= (S_{xx}(\omega)-S_{yy}(\omega))/(S(\omega)\omega^4/g^2)\\
b_2(\omega) &= 2S_{xy}(\omega)/(S(\omega)\omega^4/g^2)
\end{aligned}\right\} \tag{9}$$

Long (1980) advocates the use of the identity

$$S_{xx}(\omega)+S_{yy}(\omega)=S(\omega)(\omega^2/g)^2$$

to define ω^2/g in eqns. (9), and since this appears to have several advantages, we shall follow Long (1980) and define

$$\left.\begin{aligned}
d_1 &= S_{xh}/(S(S_{xx}+S_{yy}))^{1/2}\\
d_2 &= S_{yh}/(S(S_{xx}+S_{yy}))^{1/2}\\
d_3 &= (S_{xx}-S_{yy})/(S_{xx}+S_{yy})\\
d_4 &= 2S_{xy}/(S_{xx}+S_{yy})
\end{aligned}\right\} \tag{10}$$

In addition, we define the dispersion ratio

$$R=((S_{xx}+S_{yy})/(S^{1/2}(\omega^2/g)) \tag{11}$$

Unless $d\chi$ is confined to a surface $|\boldsymbol{k}|=k(\omega)$, the d-parameters are not Fourier coefficients of a directional distribution. Note that all the d-parameters are of such a form that they are independent of the amplitude transfer functions of heave, pitch and roll. Furthermore, d_3 and d_4 are also independent of the phase transfer functions. Thus, d_3 and d_4 and all directional parameters computed from them are completely independent of the transfer function errors for a symmetric buoy. Write for simplicity

$$\langle g(\omega)\rangle = \int_{\boldsymbol{k}} g(\boldsymbol{k},\omega)\, d\chi(\boldsymbol{k},\omega) \Big/ \int_{\boldsymbol{k}} d\chi(\boldsymbol{k},\omega)$$

Then from eqn. (7):

$$\left.\begin{aligned} d_1&=\langle k_1\rangle/\langle k^2\rangle^{1/2}\\ d_2&=\langle k_2\rangle/\langle k^2\rangle^{1/2}\\ d_3&=(\langle k_1{}^2\rangle-\langle k_2{}^2\rangle)/\langle k^2\rangle\\ d_4&=2\langle k_1k_2\rangle/\langle k^2\rangle\\ R&=\langle k^2\rangle^{1/2}/(\omega^2/g) \end{aligned}\right\} \tag{12}$$

From Schwartz' inequality it is evident that

$$\left.\begin{aligned} (d_1{}^2+d_2{}^2)&\leqslant 1\\ (d_3{}^2+d_4{}^2)&\leqslant 1 \end{aligned}\right\} \tag{13}$$

The mean wave directions θ_1 and θ_2 and spreading σ_1 for each frequency are now defined by

$$\left.\begin{aligned} \theta_1&=\operatorname{arctg}(d_2/d_1)\\ \theta_2&=\tfrac{1}{2}\operatorname{arctg}(d_4/d_3)\\ \sigma_1{}^2&=2(1-(d_1{}^2+d_2{}^2)^{1/2}) \end{aligned}\right\} \tag{14}$$

(Long 1980).

Some of these parameters, originally derived from the linear model turn out to have meaningful interpretations in the general case as well. θ_1 is simply the direction of $\langle \boldsymbol{k}(\omega)\rangle$, whereas σ_1 may be expressed in terms of $|\langle \boldsymbol{k}\rangle|$ and $\langle k^2\rangle^{1/2}$. Contrary to the spreading expressed in terms of the unnormalized Fourier coefficients given in (9), σ_1 is always defined as a result of eqn. (13).

Whereas the support of $d\chi$ and the unnormalized Fourier coefficients are substantially influenced by a current, the d-parameters show a less sensitive behaviour. Consider a wave number spectrum of the form $\psi(k,\theta)=k^{-4}D(\theta,x)$ which leads to a frequency spectrum proportional to ω^{-5} in the absence of currents. For D there are various possible choices but we choose here the Poisson kernel due to its particularly simple expression

$$D(\theta,x)=\frac{1}{2\pi}\left[1+2\sum_{n=1}^{\infty}x^n\cos n\theta\right]=\frac{1-x^2}{2\pi(1-2x\cos\theta+x^2)},\quad 0<x<1$$

In Fig. 1 the change in direction θ_1 and Poisson parameter $x=(d_1^2+d_2^2)^{1/2}$ due to current is shown. Note, for example, that $\langle k_1 \rangle$ is computed as follows

$$\langle k_1(\omega)\rangle = \int_{-\pi}^{\pi} k\cos\theta\psi(k,\theta)\left|\frac{\partial k}{\partial\omega}\right| k\,d\theta \Big/ \int_{-\pi}^{\pi}\psi(k,\theta)\left|\frac{\partial k}{\partial\omega}\right| k\,d\theta, \quad \boldsymbol{k}=\boldsymbol{k}(\theta,\omega)$$

(cf. eqn. (5)).

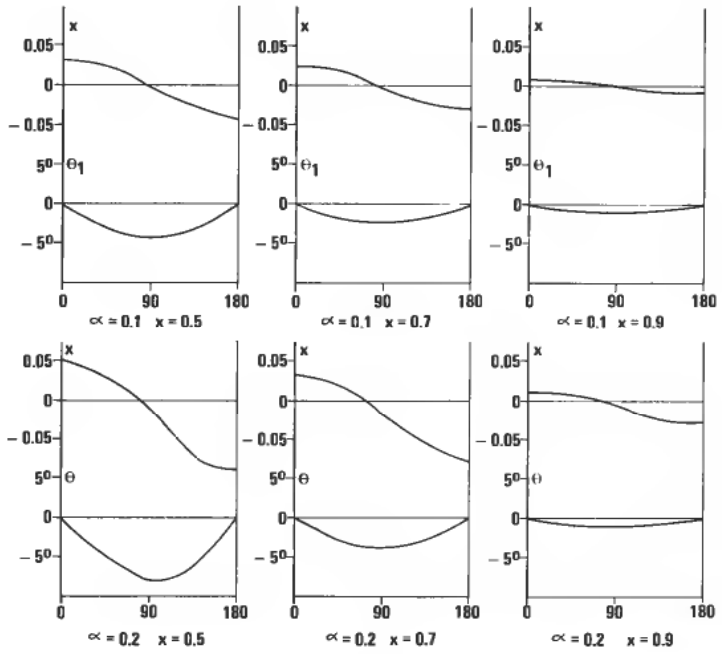

Figure 1. Change in mean wave direction θ and Poisson parameter x caused by a uniform current U, $\alpha = U\omega/g$. The angle between current and mean wave direction is shown on the abscissa.

The parameter α is the ratio between current magnitude U and the linear phase velocity g/ω, $\alpha = U\omega/g$. It is seen that at least for low frequencies, the effect of currents (with physical magnitudes) on θ_1, x, and hence for $\sigma_1=(2(1-x))^{1/2}$, is negligible. The dispersion ratio as shown in Fig. 2 is strongly influenced, however. The effect on R of a current equal to 0·5 m/s is shown in Fig. 3, for a current direction along and opposite to the mean wave direction.

Using the asymptotic properties of auto- and cross-spectra, Long (1980) derived the approximate probability distribution of the estimates $\{d_i\}$ of the d-parameters. If the spectral estimates have been computed with sufficiently many degrees of freedom, $\{\hat{d}_i\}$ will be jointly Gaussian with mean $\{d_i\}$ and a covariance matrix V which is given by Long (1980, Table 1). Although Long assumed the linear model in his derivations, it is important to note that the statistical theory applies to the general case without modification. For a valid model the quantity

$$\rho^2=(\hat{d}-d)^T V^{-1}(\hat{d}-d)$$

will be approximately χ^2-distributed with 4 degrees of freedom. This provides an acceptance/rejectance test for chosen models of the directional spectrum.

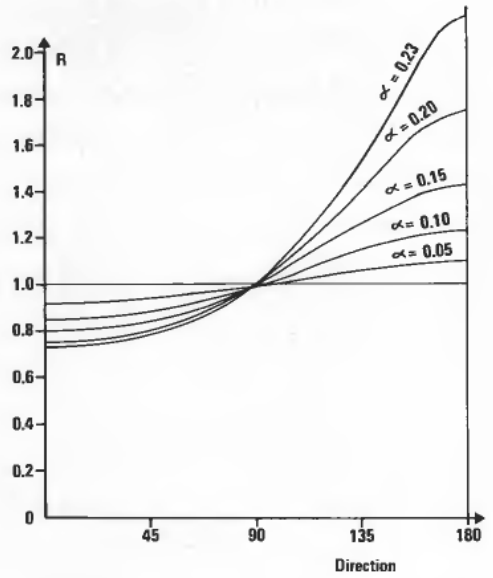

Figure 2. Variation of dispersion ratio R with $\alpha = U\omega/g$ and the angle between current and mean wave direction for $x = 0{\cdot}9$.

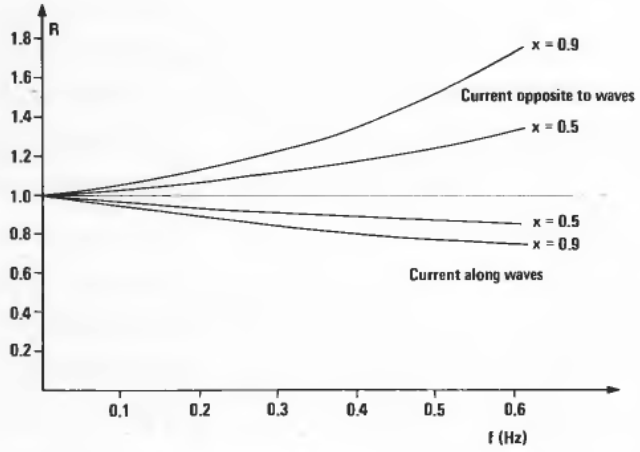

Figure 3. Change in R due to a current equal to 0·5 m/s along and opposite to the mean wave direction.

Approximate statistical properties of parameters computed from $\{\hat{a}_i\}$ may be obtained by use of the Taylor expansion technique as shown in Long (1980). We close the present section by showing an example of the variability of $\hat{\theta}_1$, $\hat{\theta}_2$, and $\hat{x}$ (Figs. 4 and 5). The width of the confidence intervals is inversely proportional to the square root of the degrees of freedom used in the spectral estimates if the bias and the deviation from the normal distribution is negligible.

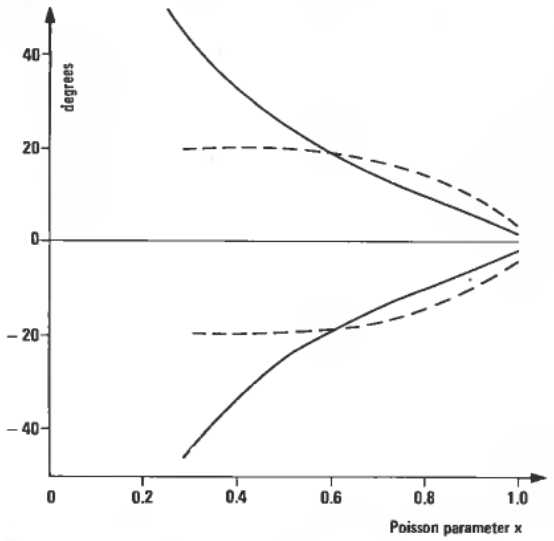

Figure 4. 90% probability intervals for $\hat{\theta}_1$ (solid line) and $\hat{\theta}_2$ (dashed line) as a function of Poisson parameter x (32 degrees of freedom).

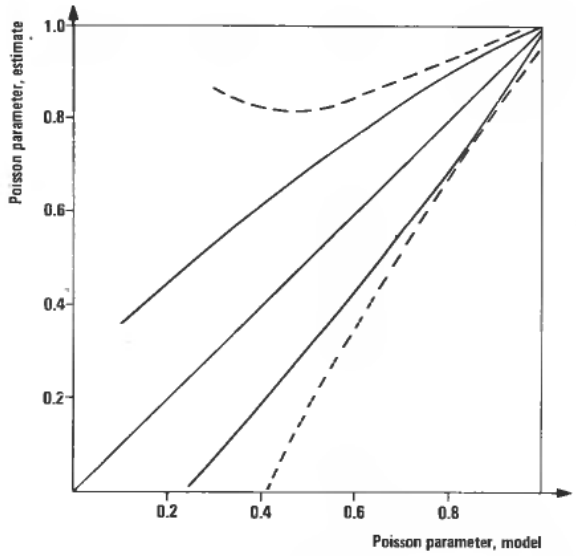

Figure 5. 90% probability intervals for $\hat{x}_1=(\hat{d}_1^2+\hat{d}_2^2)^{1/2}$ (solid line) and $\hat{x}_2=(\hat{d}_3^2+\hat{d}_4^2)^{1/4}$ (dashed line) as a function of Poisson parameter x (32 degrees of freedom).

4. The NORWAVE heave, pitch and roll buoy

The NORWAVE buoy is a medium-sized wave buoy which combines the ability to measure wave directionality with a variety of meteorological measurements. It was originally developed jointly by the Christian Michelsens Institute in Bergen and the Continental Shelf Institute in Trondheim and is now manufactured and marketed by Bergen Ocean Data. The buoy consists of a discus shaped hull of diameter 2·5 m with a cylindrical instrument section, a subsurface stabilizing steel leg with a ballast

weight and a mast for supporting meteorological sensors (cf. Fig. 6). The mooring system (Fig. 7) was designed with the aim to reduce the forces on the buoy produced by frictional, inertial and elastic mooring line effects. The buoy's instrument section contains a standard Datawell heave, pitch and roll sensor (Hippy 40), although latterly this has been replaced by the Hippy 120 for better low frequency accuracy. The time series of heave, pitch and roll as well as mean wind speed and direction, air and sea temperature and air pressure are all logged on a Sea Data digital tape recorder at a recording interval of 3 hours. The buoy is equipped with an Argos satellite transmitter which allows near real time information and has proved invaluable on a number of occasions for detecting errors and instrument malfunction. In June 1982 one of the buoys was fitted with a microprocessor which allows various wave parameters such as significant wave height and the wave frequency spectrum to be transmitted by satellite.

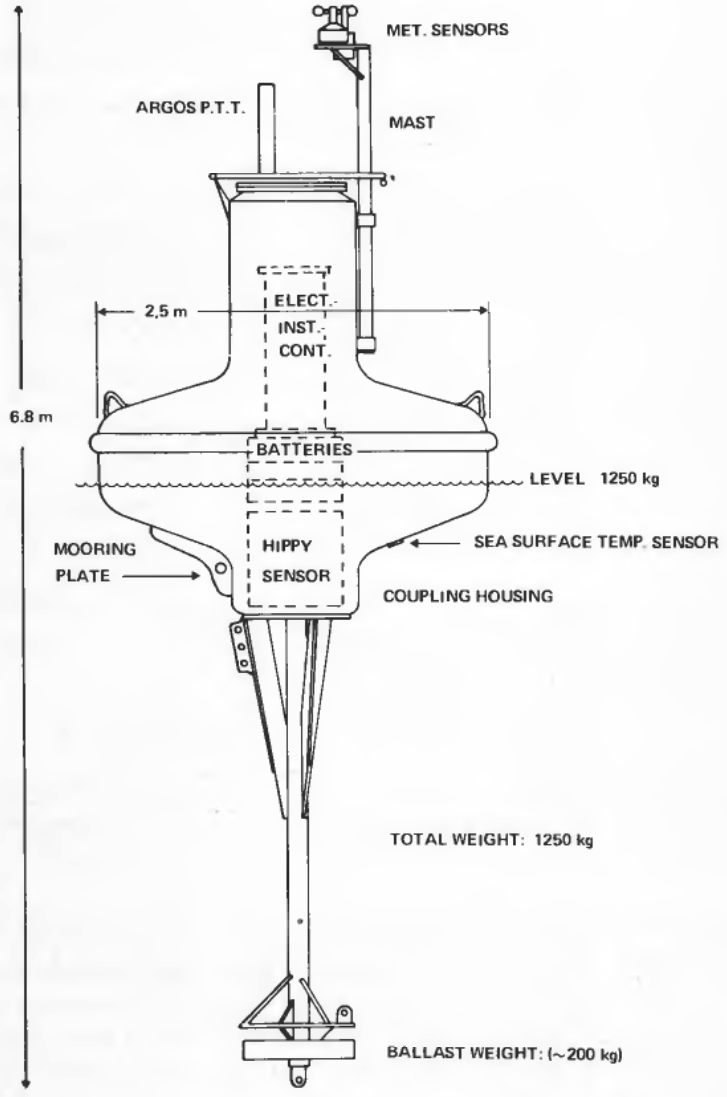

Figure 6. The NORWAVE buoy ODAS-490.

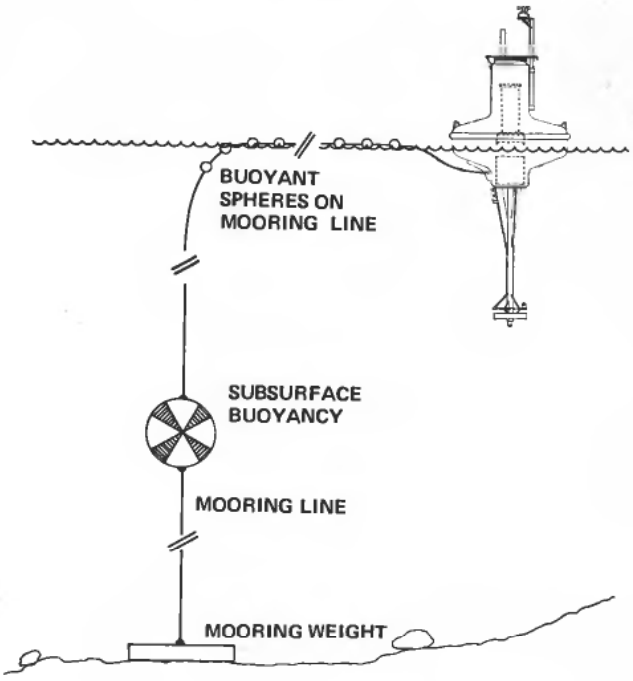

Figure 7. Typical mooring system for the NORWAVE buoys.

A series of intercalibration experiments have been carried out to cross-check the various wave and meteorological parameters measured by the buoy. A conventional Datawell Waverider was used as a reference for the heave power spectra and intercalibration of the meteorological parameters were carried out during June–September 1980 using measurements from a drilling platform which was operating nearby (Audunson *et al.* 1982).

NORWAVE buoys have now been in operation offshore Norway for 3 years so that a large data set already exists. During this period the buoys have survived under severe conditions with mean wind speeds over 32 m/s and sea states with significant wave height as high as 14 metres. Extreme waves over 20 metres have also been measured. The data set which has been used here comes from measurements with the NORWAVE buoy ODAS-490 made on Haltenbank (65°N, 7·5°E) during 1980 (Fig. 8).

No reliable calibration data exists for the directional data from the buoys, but two important corrections are implemented. Firstly, we use the manufacturer's correction for the electronic phase and amplitude distortion due to the double integration of the heave accelerometer signal. Secondly, we correct for the apparent resonance of the pitch/roll movement at around 0·3 Hz. To do this, we have assumed that the buoy behaves like a forced linear resonator in response to the surface wave slope. This works well for suitable choices of the eigenfrequency and damping ratio. The transfer function is checked from the cross-spectral phases between heave and the slopes. The best fit eigenfrequency and damping ratio turn out to be slightly dependent on the sea state. The corrections appear to work well from 0·05–0·4 Hz. However, this test strictly speaking only checks the phase of the transfer function, and in § 6 we shall see that the inferred amplitude transfer function still seems to be

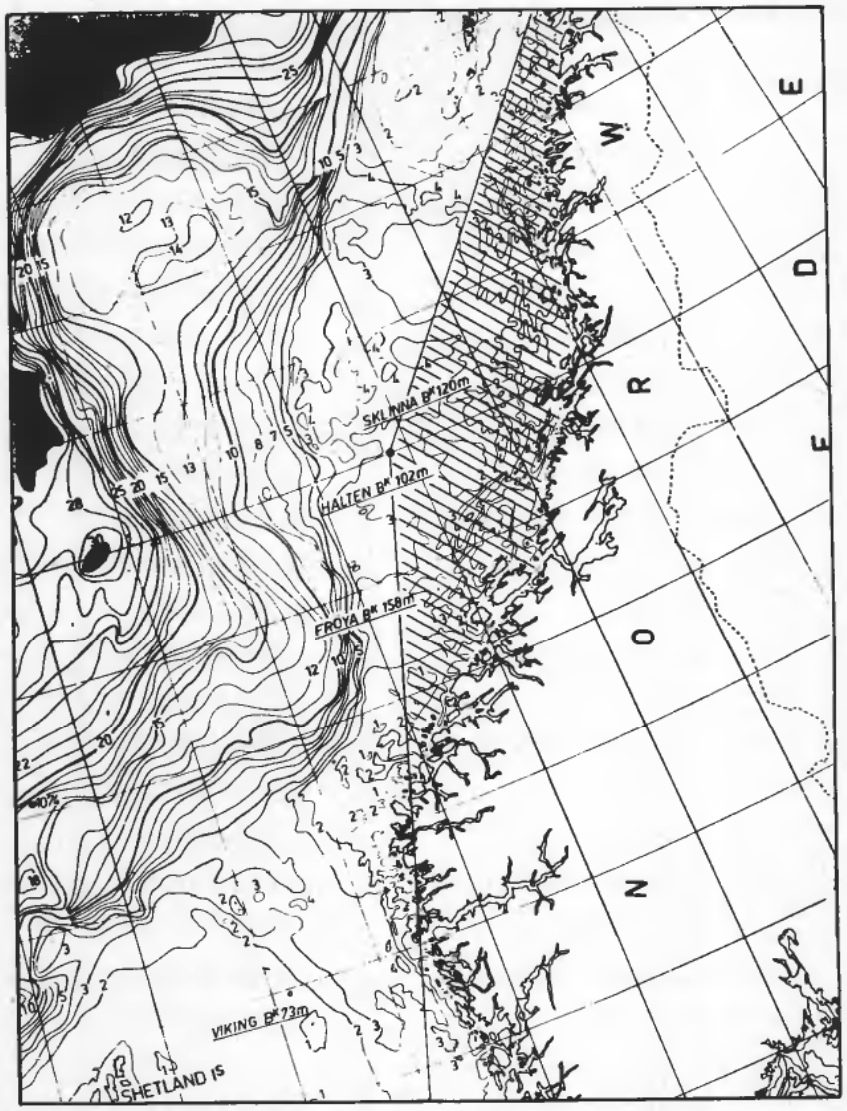

Figure 8. Map showing the measurement location at Haltenbank, and the angles predicted by the data to correspond with the coastal shadow. Shaded area signifies the fetch-limited sector.

slightly incorrect. In the following, the wind and wave directions are taken to be from the direction of origin.

In addition to internal data checks the physics provide various external checks. If we use the JONSWAP relations (Hasselmann *et al.* 1973) we find that the wind wave spectral peak is limited to frequencies above 0·14 Hz for 10 m/s offshore winds, and above 0·17 Hz for 5 m/s winds for the buoy position on Haltenbank. In Fig. 9 we have plotted the frequency of occurrence of mean wave directions for individual frequencies in three frequency bands for the December 1980 data set. In addition, the frequency of occurrence of wind directions is plotted for comparison. It is evident that for the low frequency band there are very few occurrences of mean wave direction in an arc of directions which corresponds almost exactly with that of the 'coastal

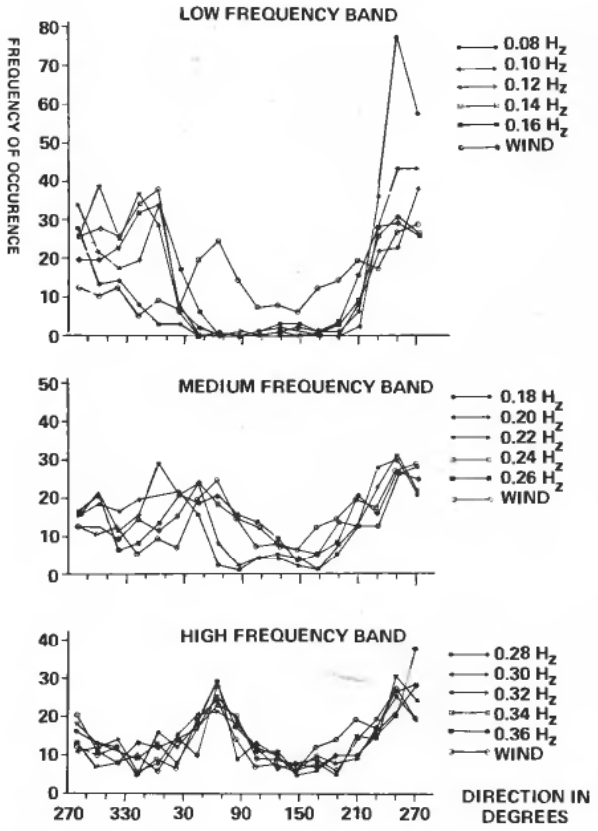

Figure 9. Frequency of occurrence plots of mean wave directions for December 1980 (249 samples).

shadow' (35°–205°) despite the fact that the wind often blows offshore (Fig. 8). The fact that the data shows the coastal shadow well at the expected directions gives added confidence to the data. In fact, the use of this data check has in the past shown up an incorrectly mounted compass.

A second external data check which may be carried out is concerned with the arriving swell at the measurement point. The wave energy at Haltenbank during the period from the 24th to the 27th December 1980 was found to be dominated by swell and this data has been analysed in more detail in order to determine whether the estimated mean wave directions may be correlated with possible generating winds as seen from the surface weather charts. This strong swell signal was easily related to the wind fields associated with a low pressure system whose centre had remained fairly stationary over Iceland from the 21st to the 25th. A weather ship to the south of Iceland had further experienced wind speeds between 30 and 45 knots for most of this period and in the general direction of Haltenbank. The swell directions measured by the buoy were found to be mainly between 230° and 250°. These directions correspond with the 'window' between the North West coast of Scotland and the Færoe Islands thus giving strength to the supposition that these waves were generated in the Northern Atlantic to the South of Iceland. A ridge line analysis (Snodgrass *et al.* 1966) has also been carried out. This is based on the fact that the energy associated with higher frequency waves propagates at a slower rate than for lower frequency

waves according to the linear deep water group velocity. Knowledge of this enables us to predict with some accuracy the distance and time of origin of the arriving swell. From the best fit ridge line it may be determined that the distance was approximately 1400 km with a time origin at 1400 GMT on the 24th. This agrees well with the weather charts. A more detailed description of the physical interpretation of the data will be published elsewhere.

Scatter plots of wind direction versus mean wave direction, θ_1, are shown for all the data from 1980 on Fig. 10. From virtually no correlation at 0·1 Hz, the correlation increases steadily up to 0·4 Hz. The remaining observed scatter is presumably due to a combination of scatter in the wind direction measurements, veering wind situations and situations where the wind is not sufficient to influence the waves below 0·4 Hz. Veering wind examples showing the time lag between the wind direction and the wave direction in various frequency bands were discussed in Audunson *et al.* (1982).

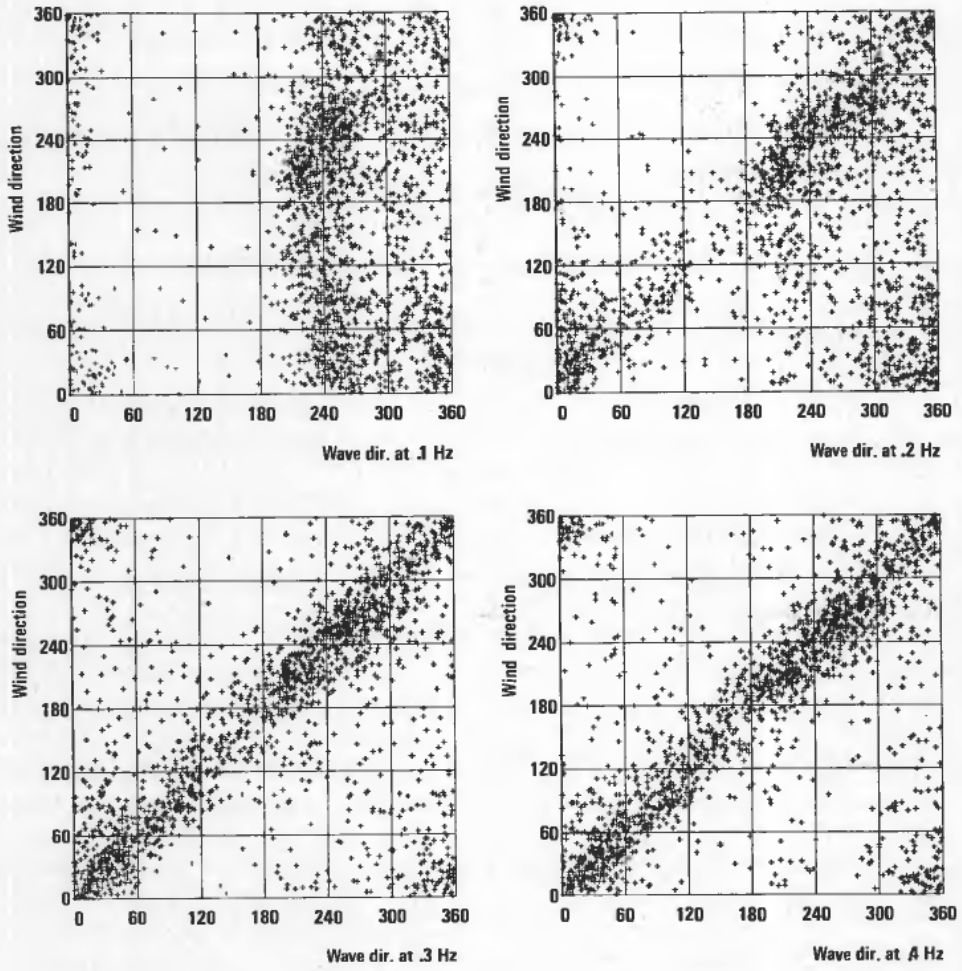

Figure 10. Correlation between wind and wave directions at various frequencies. 1851 records from 1980.

5. Directional characteristics of wave generation spectra

The frequency spectrum of a developing wind sea has been studied by numerous investigators, for example Hasselmann *et al.* (1973), and an analysis of some directional data from the JONSWAP experiment is also given in Hasselmann *et al.* (1980). The wave field will receive energy from the wind as long as the wave phase velocity is smaller than the wind velocity, i.e. for frequencies $f > f_W = g/(2\pi W)$ where W is the wind velocity (here measured at 4·2 m). For most of the data collected in the open ocean there will generally be a mixture of wave fields of different ages and directions, and in order to select a subset of data where the wind sea is predominant, only spectra where the frequency of the spectral peak, f_p, is greater than f_W are included here. Figure 11 displays the observed Poisson parameter x vs. f/f_p for $0{\cdot}5 \leqslant f/f_p \leqslant 2$ for sea states where the significant wave height is less than 2 m. The agreement with the data in Hasselmann *et al.* (1980, Fig. 3) is fairly good ($s = x/(1-x)$). When the mean and standard deviation of $\hat{x}$ are computed as a function of f/f_p an interesting fact emerges. The spreading in the estimates of x for $f > f_p$ is almost exactly equal to the inherent statistical spreading in the estimation procedure (cf. § 3) whereas the spreading for $f < f_p$ is significantly larger (Fig. 12). This should indicate that x is a unique function of f/f_p for $f/f_p > 1$. The spreading for more severe seastates (Fig. 13) is somewhat larger, however. Due to the scarcity of data, Fig. 13 contains some spectra where the wind speed is not quite as high as to ensure $f_p > f_W$.

Since x appears to be an almost unique function of f/f_p it may be of interest to look more closely into the shape of the distribution. If we denote $r_1 = (d_1^2 + d_2^2)^{1/2}$ and $r_2 = (d_3^2 + d_4^2)^{1/2}$, the Poisson distribution fulfils $r_2 = r_1^2$ whereas a wrapped normal distribution (Mardia 1972) gives $r_2 = r_1^4$. A plot showing the relationship between r_1 and $r_2^{1/2}$ for a series of common angular distributions including the $\cos^{2s}$-distribution of Longuet-Higgins *et al.* (1963), the wrapped normal and the von Mises distributions (Borgman 1979) is shown in Fig. 14. The bound $r_2 > r_1 - (2(1-r_1))^{1/2}$ is a lower bound for all positive distributions. Somewhat surprisingly none of the commonly used distributions fit the data particularly well, most measurements falling between the wrapped normal and the Poisson distribution,

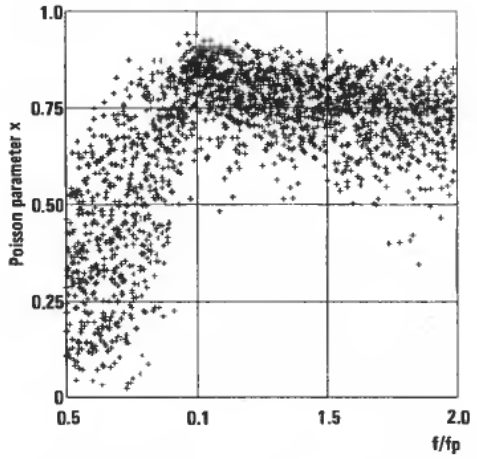

Figure 11. Observed Poisson parameter x as a function of f/f_p from 60 records with significant wave height less than 2 m and wind speed, $W > g/(2\pi f_p)$.

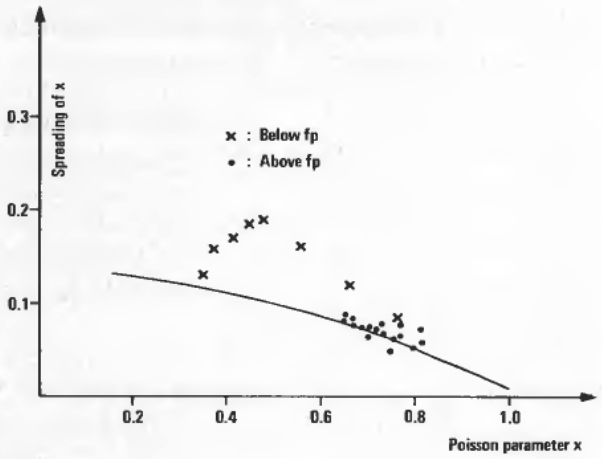

Figure 12. Observed spreading of x vs. the mean value of x for the data in Fig. 11. The solid line represents the spreading corresponding to Fig. 5.

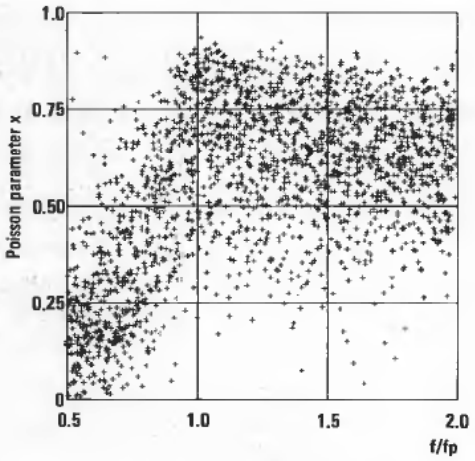

Figure 13. Observed Poisson parameter x vs. f/f_p for 60 records with significant wave height larger than 3 m and $f_p > (g/(2\pi W) - 0{\cdot}2$ Hz).

Fig. 15. Both of these distributions belong to the class of wrapped stable distributions (Mardia 1972), and a wrapped stable distribution of index $\alpha = 1{\cdot}5$ would actually fit the data reasonably well. Such a distribution has the Fourier series

$$D(\theta) = \frac{1}{2\pi}\left(1 + 2\sum_{n=1}^{\infty} x^{n^\alpha}\cos n\theta\right)$$

but unfortunately no simple closed expression for $D(\theta)$ exists. It seems probable that simpler distributions exist which fit the data equally well.

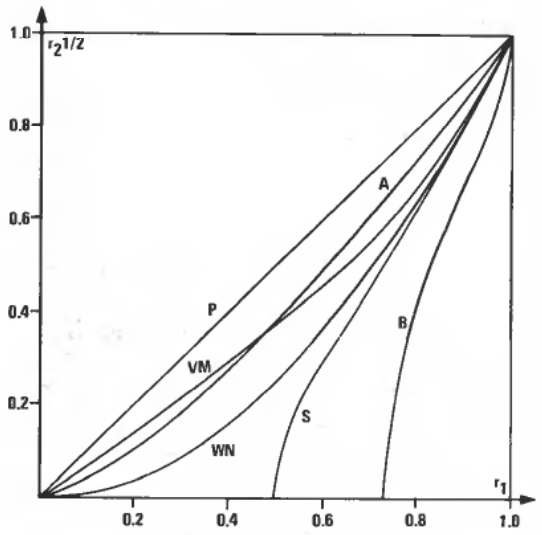

Figure 14. r_1 vs. $r_2^{1/2}$ for several directional distributions: A: wrapped stable distribution of index 1·5, B: Lower bound for $r_2^{1/2}$, P: Poisson distribution, S: $\cos^{2s}$ distribution, VM: von Mises distribution, WN: Wrapped normal distribution.

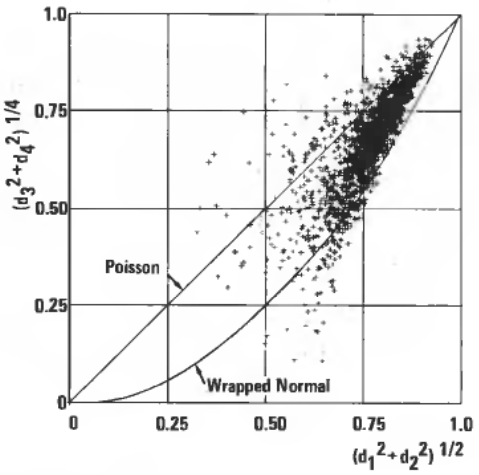

Figure 15. Observations of r_1 vs. $r_2^{1/2}$ for the records in Fig. 11. $(f > f_p)$

6. Deviations from the linear model

For heave/pitch/roll buoys deviations from the linear model are most easily detected by the root mean square wavenumber $\langle k^2 \rangle^{1/2}$, or equivalently, from the dispersion relation ratio R (eqns. 11 and 12).

Apart from the shallow water effects there are three main reasons causing this ratio to deviate from unity. First of all we have the pitch/roll response of the buoy. The NORWAVE buoys have only been checked for the phase transfer function of pitch and roll (cf. § 3). Fortunately, the d-parameters are independent of the amplitude transfer functions of pitch and roll as long as they are equal, but as is easily

seen from the definition, R is linearly dependent on the pitch/roll amplitude transfer function. The second effect that causes R to deviate from unity is current advection, also treated in § 3. Finally, there is the question of non-linear contributions to the wave field. The existence of 'bound' components in the wave field has been a question of much controversy over the last few years (Phillips 1977, Dudis 1981). It has been found, at least for steep laboratory waves that components with higher frequency than the spectral peak propagate with the phase velocity corresponding to the spectral peak frequency, that is, the wave field is non-dispersive for the higher frequencies.

However, other studies which have used buoys find the dispersion relation to be fairly well satisfied. A simple explanation of this seemingly contradictory behaviour has recently been given by Dudis (1981) who shows that the difference appears to be a question of definitions rather than physics. If we follow Dudis and consider a uni-directional spectrum of the form

$$\phi_N(\omega)\cdot\delta\left(k-\frac{\omega}{c_p}\right)+\phi_D(\omega)\cdot\delta\left(k-\frac{\omega^2}{g}\right)$$

where ϕ_N is the non-dispersive and ϕ_D the dispersive part, one can easily prove that R in this case is

$$R=\left(\frac{((g/\omega)/c_p)^2+r}{1+r}\right)^{1/2},\quad r=\phi_D/\phi_N$$

A graph of R as a function of ω/ω_p where $c_p=g/\omega_p$ is shown in Fig. 16. Note that r in general is dependent on ω. Judging from Mitsuyasu *et al.* (1979) there are cases for steep waves and frequences $\omega>2\omega_p$ where R is substantially smaller than 1.

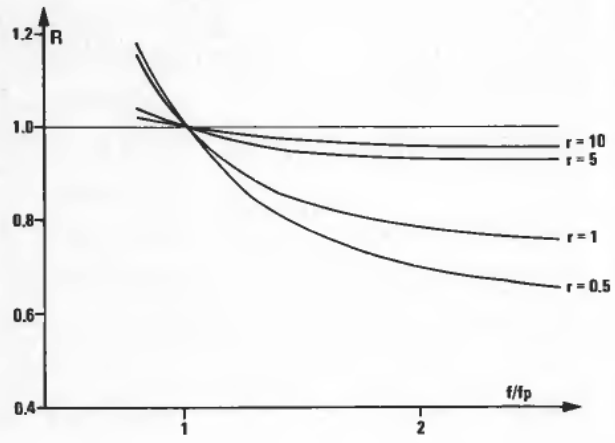

Figure 16. Variation of R for various values of $r=\phi_D/\phi_N$.

The NORWAVE data has so far not been analysed with the above mentioned effects in mind, and in what follows only very preliminary results are shown. Figure 17 shows the mean dispersion ratio for the data from March to October 1980. The data set is sorted into three groups according to significant wave height which R appears to be slightly dependent on. The somewhat puzzling behaviour around

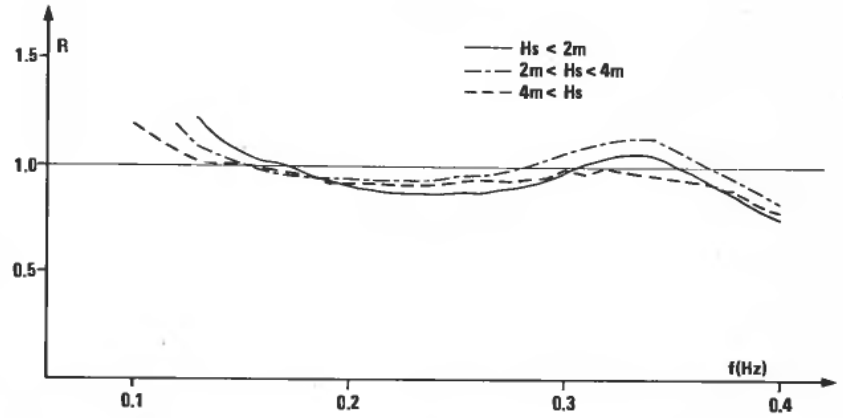

Figure 17. Mean dispersion ratio for 1400 records from March–October 1980.

0·3 Hz is almost certainly due to an imperfect pitch/roll transfer function. The drop around 0·4 Hz could of course be due to non-dispersive contributions, but may also be caused by the buoy response to the waves. Note that 0·5 Hz corresponds to approximately 6 m waves which is comparable to the buoy diameter (2·5 m). At low frequencies the ratio increases drastically above unity. A plot of R vs. the normalized frequency f/f_p is shown in Fig. 18. Below f_p it appears that $\langle k^2 \rangle^{1/2}$ is approximately constant, but since the wave spectrum itself drops very fast on the low frequency side, this effect may be caused by some kind of leakage in the estimation procedure. In Fig. 19 the mean dispersion ratio has been computed using only frequencies above f_p. Moreover, the data set is divided into two groups: March–October 1980 and November–December 1980. In fact, on 8th November, the buoy lost a 50 kg chain weight which was not subsequently replaced. This altered the buoy's pitch/roll eigenfrequency and damping (Audunson *et al.* 1982). Although the new eigenfrequency and damping ratio have been used in the present analysis, the amplitude

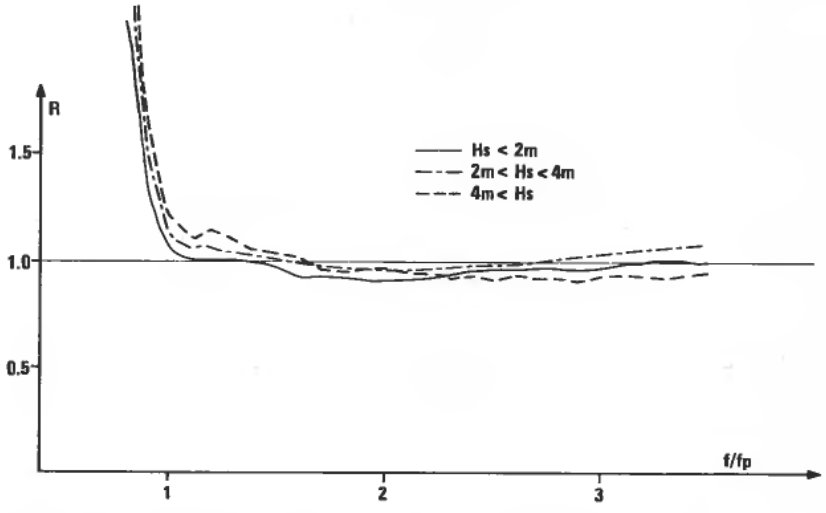

Figure 18. Same data as shown in Fig. 17 expressed in terms of f/f_p.

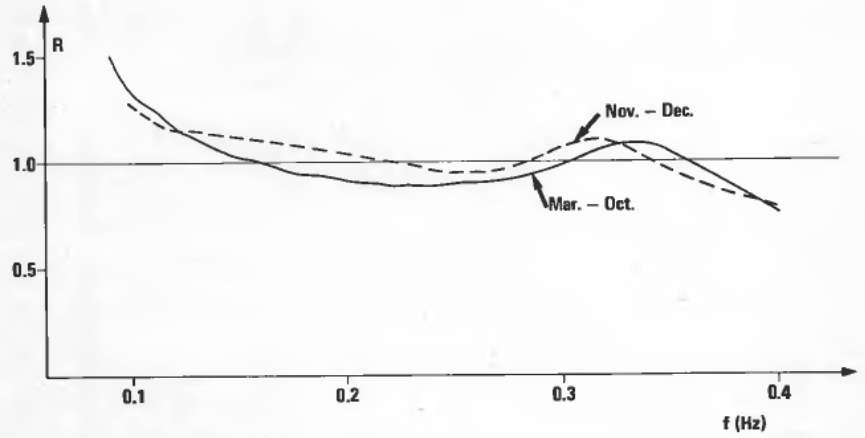

Figure 19. Mean dispersion ratio. Only including points where $f > f_p$.

transfer function still appears to be slightly incorrect. It is also a question if a linear transfer function approach is sufficient for the finer data analysis.

Current measurements were not available from the location of the buoy during 1980. The buoy is also situated at a location with small tidal currents. However, from surface current measurements carried out at IKU it has been found, in agreement with other studies, that the wind transfers a proportion of its momentum to set up a drift current with a magnitude of around 2–3% of the wind speed and in a direction approximately 45° to the right of the wind. We have therefore considered wave data collected during rather strong winds (> 5 m/s) in order to investigate the effect of wind induced currents. The results are shown in Fig. 20. For each frequency band the mean wave direction has been computed and compared with the wind direction +45°. From the graph it is apparent that the mean dispersion ratio is lower when the mean wave direction is along the current direction. The effect is not very pronounced since even a wind of 10 m/s should not produce higher currents than 0·20–0·30 m/s.

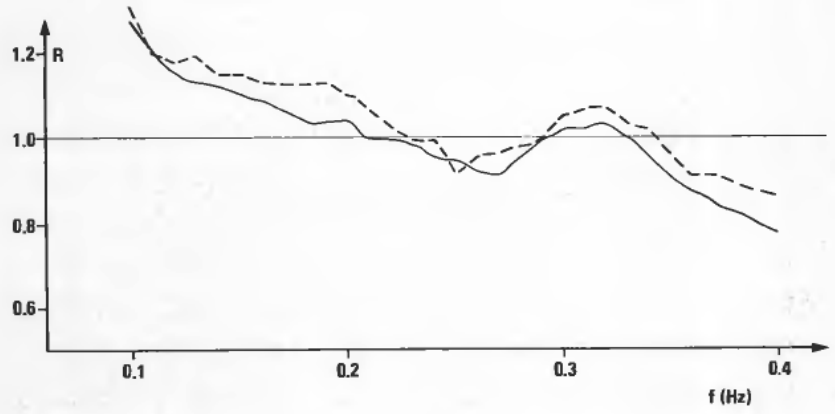

Figure 20. Mean effect of wind induced currents. Data from November and December 1980 where the wind speed is greater than 5 m/s. θ = mean wave direction, CD = wind induced current direction. ——: $|\theta - CD| < 45°$, – – –: $|\theta - CD| > 90°$.

7. Conclusion

Of the many methods to measure directional wave data, the heave/pitch/roll data buoys offer a relatively cheap method for obtaining data in remote areas. Data tests using external geographic features such as the 'coastal shadow' and remote storms have shown that the buoys will provide reliable wave directions. The spreading around the mean wave direction also appears to be consistent with other studies. The general theory indicates that the data from the buoys contains more information than is usually extracted in the conventional data analysis. The theory also gives a tool to analyse the properties of commonly used parameters under the influence of currents and non-linearities. Measured deviations from the linear model, such as those caused by currents, may well be used to measure the current magnitude and direction, but this requires further work.

Several NORWAVE heave/pitch/roll data buoys are presently operating offshore Norway where they provide long term wave data for climatological purposes as well as near real time sea state information for forecasting and operational use.

Acknowledgments

The general theory presented here was originally suggested to one of the authors (HEK) by Professor Erik Mollo-Christensen when staying at the Department of Meteorology and Physical Oceanography, M.I.T. We are indebted to Professor Mollo-Christensen for his hospitality and enlightening comments.

The wave data have been collected during the Oceanographic Data Acquisition Project (ODAP) which is financed by the Norwegian oil companies STATOIL, Norsk Hydro, and SAGA Petroleum with additional funding from the Royal Norwegian Council for Scientific and Industrial Research (NTNF) and IKU. We appreciate that all collected data is open to general use.

The preparation of this manuscript has been sponsored by NTNF through the project 'Analysis of Wave Data', 1810.7890.

References

Audunson, T., Barstow, S. F., and Krogstad, H. E. (1982). Analysis of wave directionality from a heave, pitch and roll buoy operated offshore Norway. *Proc. Int. Conf. of wave and wind directionality with application to the design of structures*, Edition Technip, Paris, pp. 87–118.

Borgman, L. E. (1979). Directional Wave Spectra from Wave Sensors. In *Ocean Wave Climate*, Ed. M. D. Earle and A. Malahoff, Plenum Press, pp. 269–300.

Dudis, J. J. (1981). Interpretation of Phase Velocity Measurements of Wind-Generated Surface Waves. *J. Fluid Mech.*, **113**, 241–249.

Forristall, G. Z., Ward, E. G., Cardone, V. J., and Borgman, L. E. (1978). The Directional Spectra and Kinematics of Surface Gravity Waves in Tropical Storm Delia. *J. Phys. Ocean.*, **8**, 888–909.

Gihman, I. I., and Skorohod, A. V. (1980). *The Theory of Stochastic Processes*, Vol. 1, Springer-Verlag, Berlin, Heidelberg, New York.

Hasselmann, K. (1962). On the Nonlinear Energy Transfer in a Gravity Wave Spectrum. *J. Fluid Mech.*, **12**, 481–500.

Hasselmann, D. E., Dunckel, M., and Ewing, J. A. (1980). Directional Wave Spectra Observed During JONSWAP 1973. *J. Phys. Ocean.*, **10**, 1264–1280.

HASSELMANN, K., BARNETT, T. P., BOUWS, E., CARLSON, H., CARTWRIGHT, D. E., ENKE, K., EWING, J. A., GIENAPP, H., HASSELMANN, D. E., KRUSEMAN, P., MEERBURG, A., MÜLLER, P., OLBERS, D. J., RICHTER, K., SELL, W., and WALDEN, H. (1973). Measurements of Windwave Growth and Swell Decay During the Joint North Sea Wave Project (JONSWAP). *Dtsch. Hydrogr. Z.* **A8** (Suppl.), No. 12.

HOGBEN, N. (1982). Directional Wave Spectra Applications 1981. *Proc. Int. Conf. of wave and wind directionality with application to the design of structures*, Edition Technip, Paris, pp. 151–166.

KITAIGORODSKII, S. A., KRASITSKII, V. P., and ZASLAVSKI, M. M. (1975). On Phillips' Theory of Equilibrium Range in the Spectra of Wind-Generated Gravity Waves. *J. Phys. Ocean*, **5**, 410–420.

LONG, R. B. (1980). The Statistical Evaluation of Directional Spectrum Estimates Derived From Pitch/Roll Buoy Data. *J. Phys. Ocean.*, **9**, 373–381.

LONGUET-HIGGINGS, M. S. (1956). On the Statistical Theory of a Random Moving Surface. *Proc. Camb. Phil. Soc., Ser A*, **237**, 212–232.

LONGUET-HIGGINS, M. S., CARTWRIGHT, D. E., and SMITH, N. D. (1963). Observations of the Directional Spectrum of Sea Waves Using the Motions of a Floating Buoy. *Ocean Wave Spectra*, Englewood Cliffs, N.Y., Prentice-Hall, Inc., pp. 111–136.

MARDIA, K. V. (1972). *Statistics of directional data*, Academic Press, London.

MITSUYASU, H., MASUDA, A., and KUO, Y.-Y. (1979). The Dispersion Relation of Random Gravity Waves, Part 1. *J. Fluid. Mech.*, **92**, 771–730.

NEWMAN, J. N. (1980). *Marine Hydrodynamics*, MIT Press, Cambridge, Massachusetts.

PHILLIPS, O. M. (1977). *The Dynamics of the Upper Ocean*, Cambridge University Press.

SNODGRASS, F. E., GROVES, G. W., HASSELMANN, K. F., MILLER, G. R., MUNK, W. H., and POWERS, W. H. (1966). Propagation of Ocean Swell across the Pacific. *Phil. Trans. Roy. Soc., London*, **A259**, 431–497.

TORSET, O. P., and OLSEN, O. A. (1982). The Need of Directionality for Structure Design. *Proc. Int. Conf. of wave and wind directionality with application to the design of structures*, Edition Technip, Paris, pp. 365–378.